Journal of Power Sources 293 (2015) 101–108

Contents lists available at ScienceDirect

Journal of Power Sources

journal homepage: www.elsevier.com/locate/jpowsour

On the synthesis of nickel oxide nanoparticles by sol–gel technique and its electrocatalytic oxidation of glucose

Amgad S. Danial [a], M.M. Saleh [b, c, **], S.A. Salih [b], M.I. Awad [b, d, *]

[a] Ministry of Military Production, Cairo, Egypt
[b] Department of Chemistry, Faculty of Science, Cairo University, Cairo, Egypt
[c] Chemistry Department, College of Science, King Faisal University, Al-Hassa, Saudi Arabia
[d] Chemistry Department, Faculty of Applied Sciences, Umm Al-Qura University, Makkah Al Mukarramah, 13401, Saudi Arabia

HIGHLIGHTS

- Nano-NiO_x of peculiar shape is prepared and applied for glucose electrocatalysis in 0.3 M KOH.
- Calcination temperature and nano-NiO_x loading played a crucial role in electrocatalysis.
- Highest activity is obtained at loading 0.08 mg cm^{-2} and calcination temp. 200 °C.

GRAPHICAL ABSTRACT

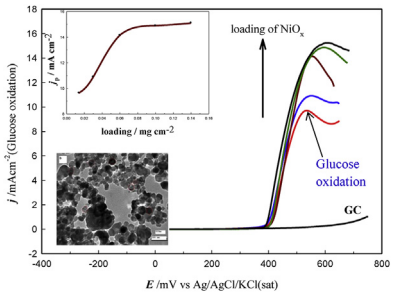

ARTICLE INFO

Article history:
Received 2 February 2015
Received in revised form
5 May 2015
Accepted 10 May 2015
Available online

Keywords:
Metal oxide
Nanoscale nickel oxide
Sol–gel technique
Electrocatalysis
Glucose

ABSTRACT

Nickel oxide nanoparticles (nano-NiO_x) of peculiar shape are prepared by sol–gel technique and its electrocatalytic activity is evaluated at different conditions. The thus prepared nanoparticles are annealed at three different temperatures, *i.e.,* 200, 400 and 600 °C and anchored on glassy carbon (GC) electrode. Nano-NiO_x modified GG (nano-NiO_x/GC) electrodes are subjected to surface analysis techniques such as field emission scanning electron microscopy (FE-SEM) high resolution transmission electron micrograph (TEM) and X-ray diffraction (XRD). Electrochemical characterizations are performed using cyclic voltammetry and *chronoamperometric* techniques. The effects of annealing temperature on the morphological structure, surface concentration and subsequently on the electrochemical properties of nano-NiO_x/GC are examined. Experimental results indicate that the grain size and electrochemical characteristics of the nano-NiO_x/GC are significantly affected by the annealing temperature. The electrocatalytic oxidation of glucose at nano-NiO_x/GC electrode is significantly enhanced especially with nano-NiO_x annealed at 200 °C compared to those annealed at 400 and 600 °C. Nano-NiO_x is believed to play a crucial role as a catalytic mediator to facilitate the charge transfer during the oxidation of glucose.

1. Introduction

Metal oxide nanoparticles have been recently used for several applications because of their superior properties [1–6]. Preparation of such materials includes dry and wet techniques [7–14]. Sol–gel technique is one of the widely used techniques [15–19] in

* Corresponding author. Chemistry Department, Faculty of Applied Sciences, Umm Al-Qura University, Makkah Al Mukarramah, 13401, Saudi Arabia.
** Corresponding author. Chemistry Department, College of Science, King Faisal University, Al-Hassa, Saudi Arabia.
E-mail addresses: mahmoudsaleh90@yahoo.com (M.M. Saleh), mawad70@yahoo.com (M.I. Awad).

http://dx.doi.org/10.1016/j.jpowsour.2015.05.024
0378-7753/

preparation of metal oxide nanoparticles as it is simple and cost effective. Also, the prepared materials have attractive properties like electrical, optical, magnetic and mechanical properties. Metal oxide nanoparticles are considered to be a host of other properties for various useful applications in diverse fields. The development of sol–gel synthesis methods for transition metal oxides coincided with a growing interest in using nanoparticles of transition metal oxides as catalysts for alcohol and sugar oxidation, medical applications, wastewater treatment and food industry. Metal oxides are usually prepared at different calcination temperatures and it has been reported that the annealing temperature has dramatic effects on the particle size and on the specific area of the prepared powder [20–23].

Structural modifications include changes in surface geometry (crystal planes, clusters, adatomes), and variations in the electronic state of the catalyst material. On the other hand the electrooxidation of glucose has attracted a lot of interest due to its potential application in several areas, such as the development of blood sugar sensors and fuel cells [24]. Glucose electrooxidation was firstly studied about one hundred years ago in a sulfuric acid electrolyte using a lead electrode [25]. Subsequently, it was discovered that the electrooxidation of glucose depends highly on electrode materials [26] and the crystalline orientation of their surfaces. Glucose oxidation is most active in alkaline solutions [27,28]. Several studies regarding the electrocatalysis of glucose oxidation using transition metal oxides including both bulk and nanostructures-based electrodes, such that NiO_x [29,30], CuO [31], and MnO_2 [32] have been reported.

The aim of this work is to use sol–gel technique to fabricate nanostructured material of nickel oxide (nano-NiO_x) with outstanding technological applications such as electrocatalysis for glucose oxidation. The fabricated nickel oxides nanoparticles will be morphologically and electrochemically characterized. The effects of the annealing temperature on the morphology and electrocatalytic properties of NiO_x are also examined.

2. Experimental

All chemicals used in this work were of analytical grade. They were purchased from Fisher and Sigma Aldrich and were used as received without further purification. All solutions were prepared using second distilled water.

2.1. Preparation of nickel oxide nanoparticles

For the preparation of nickel oxide nanoparticles, 5.8 g of nickel nitrate ($Ni(NO_3)_2.6H_2O$) and 4.2 g of citric acid ($C_6H_8O_7.H_2O$) were, respectively, dissolved completely in 100 ml of deionized water. Then the nickel nitrate solution was dripped in the citric acid solution. The mixed solution was heated to 70 °C with mechanical stirring for about 12 h. After the removal of water through evaporation, a translucent green gel was formed. Next, the gel obtained was aged and dried at 110 °C for 24 h; subsequently, divided into three samples (sample 1, 2 and 3), then samples were calcined at three different temperatures, *i.e.*, 200 °C, 400 °C and 600 °C (for samples 1, 2 and 3, respectively). For sample calcination, the oven temperature was adjusted and left until it reached to the desired temperature, *i.e.,* 200 °C, 400 °C and 600 °C, and then the sample was introduced to the oven and kept at this temperature (calcinated) for 4 h.

A suspension of NiO_x nanoparticles (nano-NiO_x), for being anchored on GCE, was prepared by adding the proper mass of the nano-NiOx powder in a test tube containing 5 ml ethanol + one drop of Nafion solution (5% in water). The above mixture was sonicated for 30 min in an ice bath.

2.2. Electrode modification

Glassy carbon electrode, used here as the underlying substrate for nickel oxide nanoparticles, is cleaned by mechanical polishing with aqueous slurries of successively finer alumina powder (down to 0.06 μm), then washed thoroughly with second distilled water and then ethanol. Next, 50 μL of a freshly prepared nano-NiO_x suspension (prepared as given above) is casted onto the thus cleaned GC electrode and left overnight for drying in air. The prepared loading extents, by casting different volumes of the nano-NiOx suspension, used here in this work are 0.13, 0.028, 0.057, 0.10 and 0.14 mg cm^{-2}.

2.3. Electrochemical measurements

Electrochemical measurements were performed using an EG&G potentiostat (model 273A) operated with E-chem 270 software. All measurements were performed at room temperature (25 °C). An electrochemical cell with a three-electrode configuration was used in this study. A platinum spiral wire and an Ag/AgCl/KCl (sat.) were used as counter and reference electrodes, respectively. All potentials are given with respect to this reference electrode. The working electrode was glassy carbon (diameter = 3.0 mm). A field emission scanning electron microscope, FE-SEM, (QUANTA FEG 250), high resolution transmission electron micrograph, TEM and X-ray diffraction, XRD (PANalytical, X'Pert PRO) operated with Cu target ($\lambda = 1.54$ Å) were used to identify the crystallographic structure of the nano-NiO_x.

3. Results and discussion

3.1. Structure and morphological properties

Fig. 1 shows SEM images of nano-NiO_x prepared by a sol–gel technique described in the experimental section. Calcination temperatures are (image a) 200 °C, (image b) 400 °C, and (image c) 600 °C. It can be clearly observed that nanoparticles size grew as the calcination temperature increased. In the sample calcined at 200 °C (image a), the particles seems to form an aggregation of irregular shape. The agglomeration of particles could be attributed to the extra small individual particle size which is of high surface energy [33,34]. The particle size of the aggregated particles is estimated to be ~10 nm. Increasing the calcination temperature to 400 °C (image b), leads to the formation of spherical nanoparticles of size around 20 nm. When the calcination temperature increased to 600 °C a NiO_x nanoparticles of about 42 nm is formed pointing to the crucial role of the calcination temperature on the morphological structure of the NiO_x particles. Thus, nano-NiO_x prepared at annealing temperature of 200 °C have the smallest particle size and that annealed at 600 °C have the largest particle size.

The crystallinity and purity of the NiO_x samples were evaluated based on X-ray diffraction (XRD) patterns. Fig. 2 shows such patterns of NiO_x calcined at 200 °C (a), 400 °C (b) and 600 °C (c). In spectrum (a) nano-NiO_x calcined at 200 °C is amorphous. In spectrum (b) obtained for the sample calcined at 400 ^{O}C, the XRD pattern consists of two sets of peaks, which are respectively corresponding to the nano-NiO_x. For the sample calcinated at 600 ^{O}C several peaks are obtained for the evaluated crystalline product [34].

The characteristic peaks of NiO_x appeared at $2\theta = 37.20°$, 43.20°, 44.4°, 51.7°, 62.87°, 75.20°, 76.2° and 79.38° can be readily indexed as (101), (012), (111), (200), (110), (113), (220) and (202) crystal planes of the bulk NiO, respectively. Those peaks are indexed to the face-centered cubic (FCC) crystalline structure of NiO in accordance with that of the standard spectrum (JCPDS, No. 04-0835) [35]. The

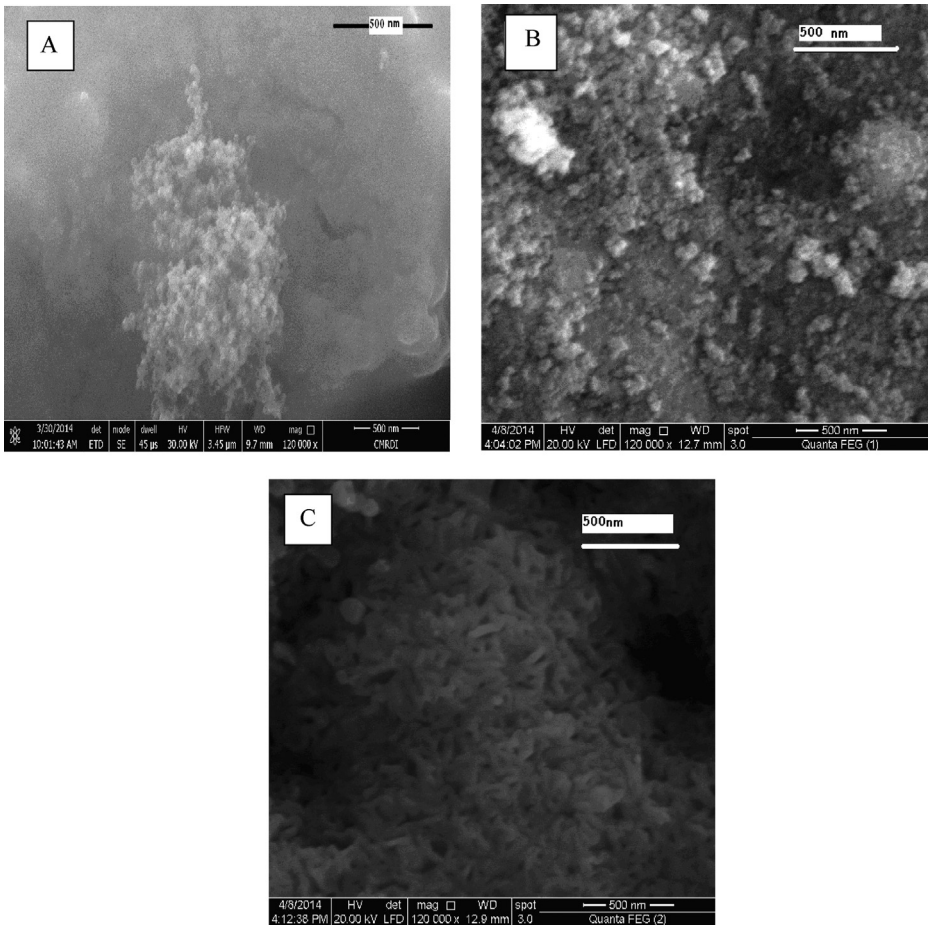

Fig. 1. FE-SEM images of nano-NiO_x. Nano-NiO_x samples were calcined at (A) 200, (B) 400 and (C) 600 °C.

XRD pattern shows that the samples are single phase structure. The average grain size D is estimated by means of the Scherrer formula [36].

$$D_{hkl} = k\,\lambda / \beta \cos\theta \quad (1)$$

where, D_{hkl} is the Average crystallite size, k is a constant shape factor ≈ 0.9, β is the full width at half maximum, λ is the wavelength of the X-ray radiation, θ is the angle of diffraction.

The average crystallite size D_{hkl} is estimated to be 26 and 50 nm at 400 °C and 600 °C, respectively. We could not estimate the particle size of nano-NiO_x calcined at 200 °C since it shows amorphous structure. No peaks of impurity were found in the XRD pattern, indicating that nanocrystalline NiO_x obtained via this synthesis method consists of pure phase. In Fig. 2, the peak sharpness and intensity increased with increasing the calcination temperature indicating an improvement of the crystallinity of the samples accompanying the crystal growth. It is obvious that upon calcination at higher temperature (600 °C), the crystallite size progressively increases with the crystal growth of the samples.

Fig. 3 shows TEM micrographs of NiO_x particles calcined at (a) 200, (b) 400 and (c) 600 °C. Determining the particle size by TEM is advantageous over XRD as the TEM is not affected by experimental errors and/or other properties of the particles such as strain or a distribution in the size. As can be seen spherical shape is exhibited by the nano-NiO_x that were calcinated at 200 °C. However, the nanoparticles calcinated at 400 and 600 °C were found to have nearly both hexagonal/cubic particle shape and hexagonal shape, respectively. A slight tilting in the lattice angle can be attributed to the non-stoichiometric composition of the oxide powder produced during the production procedure. The number of hexagonally shaped nanoparticles (nano-NiO_x) increased as the calcination temperature increased. The average particle size of the nano-NiO_x calcinated at temperatures of 200, 400 and 600 °C is estimated to be about ≈5.3, 17.3, 38 nm, respectively. There was a ≈25% variation between the TEM and XRD results for particle size due to the surface effect which is considered in TEM but not in the XRD measurements.

The selected-area electron diffraction (SAED) patterns are inserted in Fig. 3 as image a1, b1, and c1 for the samples calcinated at 200, 400 and 600 °C, respectively. The amorphous structure of the sample (200 °C) is evident from the SAED image (a1) which displayed a series of diffractional circles indicative of typical amorphous structure [37]. In case of samples calcined at 400 and 600 °C (b1 and c1, respectively), in the other hand, these diffractional circles disappeared and only separated bright dots were observed, which demonstrated the crystallization of the NiO_x samples. The above finding is in agreement with the XRD analysis.

3.2. Electrochemical characterization

Modified electrodes calcined at 200, 400 and 600 °C were electrochemically characterized by recording CVs at different scan rates (data are not shown). Before recording CVs the potential of electrodes were cycled in KOH solution. Cycling of potential in KOH

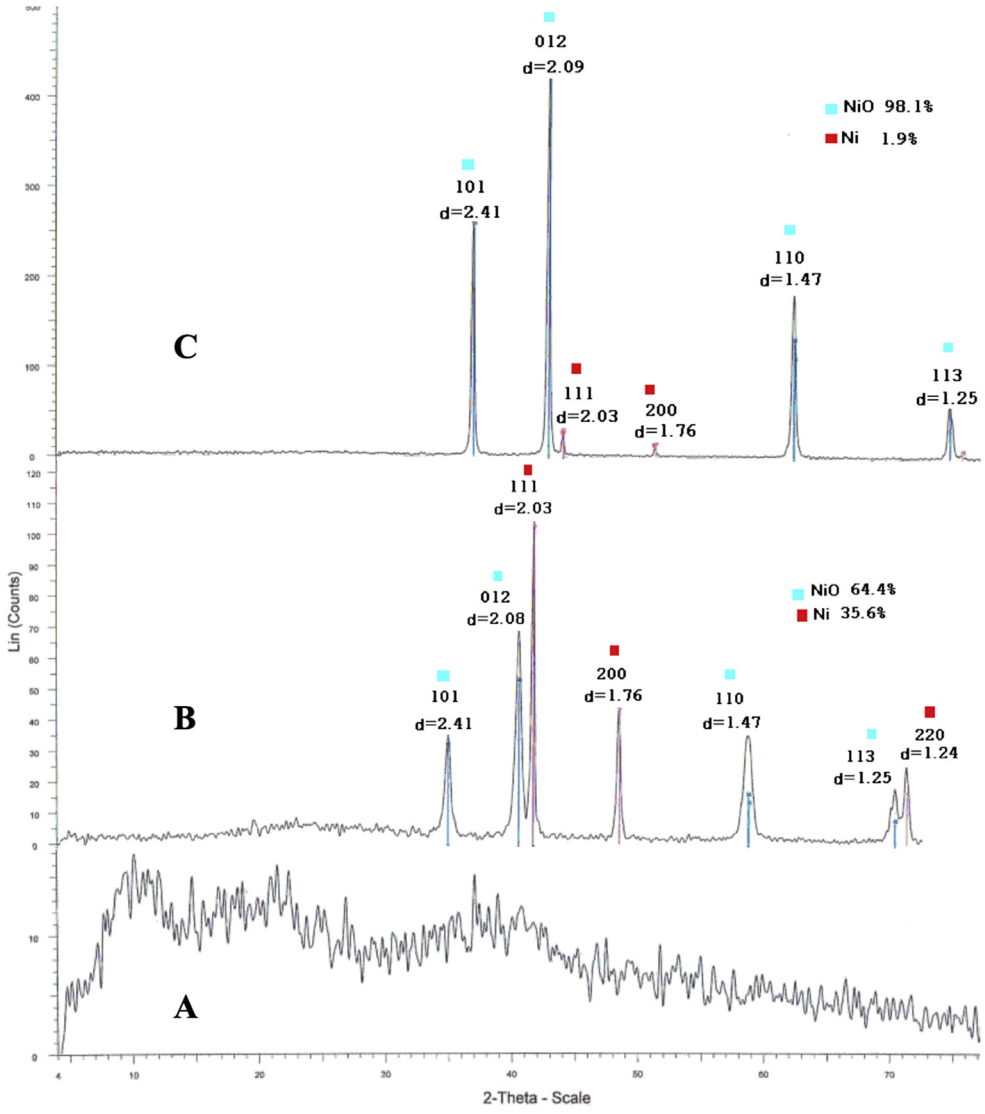

Fig. 2. X-ray diffractograms of nano-NiO_x samples calcined at (A) 200, (B) 400 and (C) 600 °C.

solution resulted in increasing the anodic and cathodic peak currents for nickel oxide species and sharpening the peaks. Cycling of potential was continuing until steady behavior and stable CVs were obtained. The characteristic redox peaks of $NiOOH/Ni(OH)_2$ were obtained in the potential range of 0.35–0.45 V [38,39]. The value of the peak current of the anodic and cathodic sweeps has the order: 200 °C > 400 °C > 600 °C. This may be attributed to the differences in the particles size of the nano-NiO_x which give rise to differences in the electronic and geometric effects and hence enhancement in the charge transfer during the Ni(II)/Ni(III) redox transition. According to the theory of quasi-reversible system, the latter redox process is a quasi-reversible process according to the following findings: j_p increases with $\nu^{1/2}$ but not in a linear manner (the $j_p - \nu^{1/2}$ is linear only at low scan rates (data are not shown here)), ΔE_p is higher than that of $59/n$ mV expected for a reversible system and ΔE_p increases with the scan rate [40]. The anodic and cathodic peak currents, j_p and j_c show straight line relations with the scan rate, ν indicating a typical behavior for the surface confined redox transformation. The values of the cathodic and anodic peak potentials were found to shift towards negative and positive directions, respectively (*i.e.*, peak separation increases) with increasing the scan rate.

The dependence of j_p on the scan rate, ν may be attributed to electrochemical activity of immobilized redox couple at the surface of the nano-NiO_x/GC electrode. The surface coverage, Γ of nickel oxide species was estimated by integrating the area under the anodic peak of the redox $Ni(OH)_2/NiOOH$ [41]:

$$\Gamma = \frac{Q}{nF} \tag{2}$$

where Q is the charge density in coulombs/cm^2. The surface concentration was estimated for the three electrodes (200, 400 and 600 °C), using Eq. (2) to be 2.25×10^{-8}, 1.68×10^{-8} and 1.10×10^{-8} mol cm^{-2} for nano-NiO_x annealed at 200, 400 and 600 °C, respectively. It is noticed from the above values of Γ that the surface concentration of NiO_x species increases with decreasing the annealing temperature. We may conclude that despite the equal amount of loading of nano-NiO_x on the electrode surface, the concentration of electrochemical active species depends on the annealing temperature. That is to say, at lower particle size (at 200 °C), there is an increase in the corners, edges and defects on the NiO_x surface which results in higher electrochemical activity of NiO_x species. The above values of Γ were used to estimate the

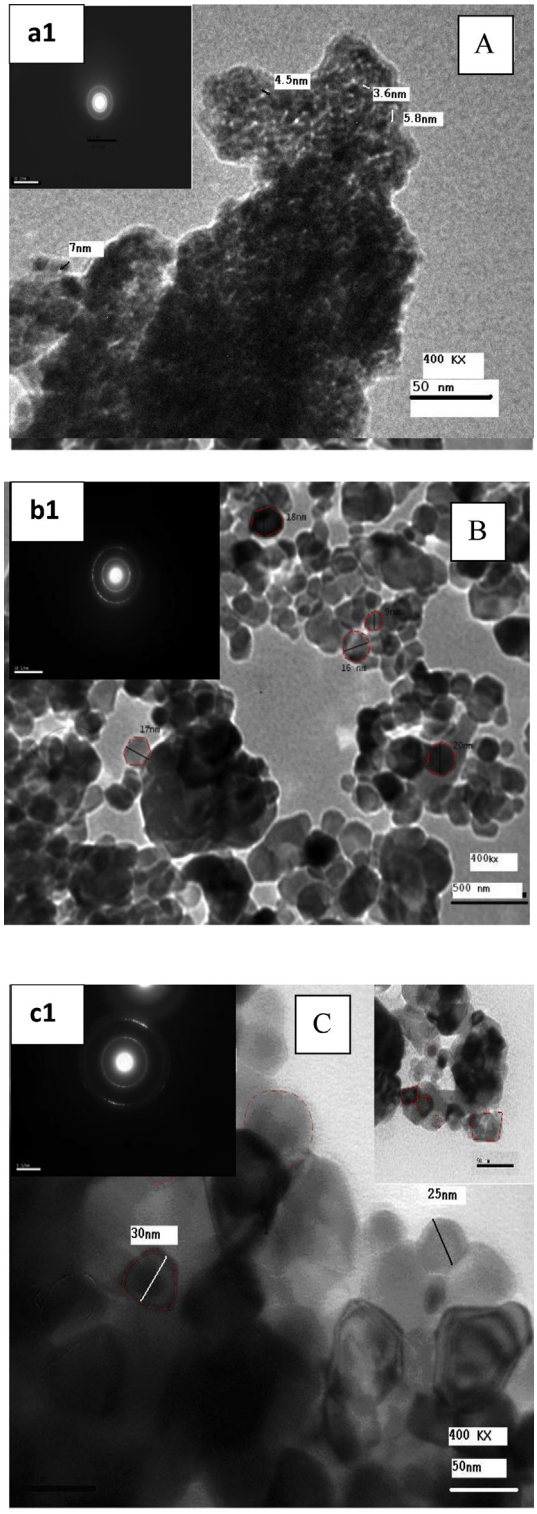

Fig. 3. TEM images of nano-NiO_x. The samples were calcined at (A) 200, (B) 400 and (C) 600 °C.

loading of $Ni(OH)_2$ at the different temperatures by using the relation; {loading (mg cm^{-2}) = Γ * Molar mass of $Ni(OH)_2$*10^3}. The loading estimated from the mentioned approach was found to be 2.08×10^{-3}, 1.56×10^{-3} and 9.8×10^{-4} mg cm^{-2} at 200, 400 and 600 °C, respectively. The utilization percentage, *UP* can be defined as:

$$UP = \frac{Estimated\ \ loaing}{Acutal\ \ loading} \times 100 \quad (3)$$

The actual loading as given above is 0.028 mg cm^{-2}. In this case, *UP* was estimated to be 7.42, 5.57 and 3.5% which points to the surface nature of the process.

3.3. Electrocatalytic characteristics

Glucose oxidation in alkaline solution is used here as a probing reaction to test the electrocatalytic characteristics of the prepared nano-NiO_x. Fig. 4 shows the cyclic voltammetry responses of (a, b) bare and (c, d) nano-NiO_x/GC electrodes at a scan rate of 100 mV s^{-1} in 0.3 M KOH both in the absence (a,c) and presence (b, d) of 10 mM glucose. The loading of NiO_x is 0.028 mg cm^{-2} at annealing temperature of 200 °C. At the bare GC electrode, the CV does not show any features in blank (curve a) and the current is slightly increased in the presence of glucose at high potential (curve b). The electrochemical behavior of the glassy carbon electrode modified with electrochemically deposited nickel oxide (NiO_x/GC) has already been reported in the literature [42–45].

At nano-NiO_x/GC electrode, a well-defined redox peaks for the $Ni(OH)_2$/NiOOH couple, centered at a potential ca. 0.45 V is obtained (curve c). In the presence of glucose (curve d), a tremendous increase in the current and a well-defined peak for glucose oxidation is obtained. Note that while the anodic peak increases, the cathodic peak of NiOOH reduction diminishes and also the peak potential of glucose oxidation shifted to more positive value. This may indicate a typical electrocatalytic process. The onset potential of the glucose oxidation is obtained at around 0.35 V. The enhancement of the glucose oxidation is attributed to the higher reactivity of the nano-NiO_x, and there are two possible reasons responsible for its reactivity. The first: the physical and chemical properties of NiO_x such as adsorption. One other reason can be discussed by considering the different forms of NiO_x. The NiO_x has two forms, stoichiometric (green in color) and non-stoichiometric (black in color); the non-stoichiometric NiO_x is more active in catalytic activity and more conductor. The oxidation state under oxygen-rich reaction is only slightly lower, which makes the redox couple Ni(II)/Ni(III) more probable for glucose oxidation by oxygen. Ni(III)-O bond energy is lowered and meanwhile Ni(III) ions quickly reduced into Ni(II) ions, therefore easily forming a redox cycle of Ni(II)/Ni(III). The hybridization between d-orbital of Ni and p-

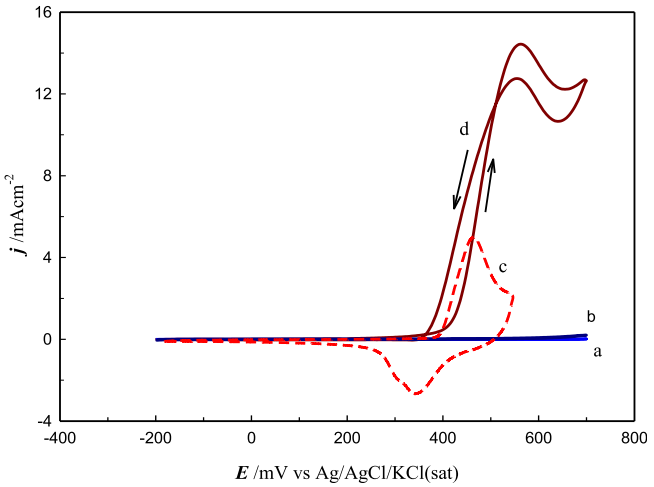

Fig. 4. CVs for (a, c) bare GC and (b, d) nano-NiO_x/GC in (a, b) 0.3 M KOH containing (c, d) 10 mM glucose. NiO_x was calcined at 200 °C.

orbital of oxygen explain the metallic conductivity in this compound [46,47]. In curve d, in the back scan anodic peak is observed. It has been reported that this peak corresponds to the oxidation of glucose at electrode free from poisoning of the oxidation product [48,49]. In the reverse half cycle, after removal of the poisoning species at high anodic potentials, the glucose is oxidized passing through a maximum. In fact the appearance of reverse anodic peak is a distinct feature of the electrocatalytic oxidation of hydroxyl-containing compounds.

Fig. 5 depicts LSV (linear sweep voltammetry) responses of Nano-NiO_x/GC in 0.3 M KOH containing 10 mM glucose at a scan rate of 100 mV s^{-1}. The NiO_x was annealed at 200 (curve b), 400 (curve c) and 600 °C (curve d). Curve a, in the other hand, shows LSV for bare GC under the same conditions. Fig. 5 demonstrates that the peak current for glucose oxidation increases as the annealing temperature decreases. This can be discussed in the light of structural properties discussed above for the SEM and TEM images. As shown above (Figs. 1–3) the particle size of NiO_x annealed at 200 °C has lower size than that obtained at 400 and 600 °C. The smaller size of NiO_x has better electrocatalytic properties due to electronic and surface enhancement of the smaller particle size. Such an enhancement with decreasing the particle size may be attributed to a stronger binding of the adsorbed glucose to the NiO_x of smaller particle size due to the low-coordination NiO_x sites such as corners, edges and defects [50]. Similar enhancement of metal oxide based catalysts due to the decease in the particle size at lower calcination temperature is reported in literature [51].

The results indicated that nano-NiO_x/GC modified electrodes can catalyze the electrooxidation of glucose to gluconolactone [52] due to the existence of Ni (II) ions according to the following reactions:

$$2Ni\ (II) \rightarrow 2Ni\ (III) + 2e^- \quad (4)$$

$$2Ni\ (III) + glucose \rightarrow 2Ni\ (II) + gluconolactone \quad (5)$$

The redox transition of nickel species from Ni (II) to Ni (III) occurs, and then in a next step glucose is oxidized on the modified surface.

$$NiO(OH) + glucose \rightarrow Ni(OH)_2 + glucolactone \quad (6)$$

Optimization of catalyst loading is an important parameter for many applications such as fuel cells and biosensors. The effects of the loading extent of NiO_x on the electrocatalytic oxidation of glucose at the modified electrodes have been investigated at calcination temperature of 200, 400 and 600 °C. NiO_x is responsible for the electrocatalytic oxidation of glucose due to presence of the Ni(II)/Ni(III) redox couple; so small loadings of the NiO_x on the GCE results in a significant enhancement in the electrocatalytic oxidation of glucose as show in Fig. 6. The latter shows LSV responses of Nano-NiO_x/GC in 0.3 M KOH solution containing 10 mM glucose at a scan rate of 100 mV s^{-1}. The loading extent slightly shifts the onset potential to less positive values but markedly increases the peak current of glucose oxidation. This can be summarized in the inset of Fig. 6. Inset shows that as the loading extent increases the peak current of glucose oxidation increases before it reaches constant value at loading extent ≥0.06 mg cm^{-2}. It may be concluded that a loading extent of 0.08 mg cm^{-2} is a proper loading of the NiO_x at the prevailing experimental conditions.

Fig. 7A shows LSV responses of nano-NiO_x/GC, annealed at 200 °C, in 0.3 M KOH containing 20 mM glucose at various scan rates. The peak potential for the catalytic oxidation of glucose shifts to increasingly positive potentials with increasing scan rate as a characteristic of irreversible voltammetric behavior. It is worth mentioning that, in the present study, in all electrochemical investigations, a strong supporting electrolyte (KOH) of relatively high concentration (0.3 M) was employed; thus, the possibility of potential shift to more positive values due to higher ohmic drop is expected to be negligible. Meanwhile, the anodic peak current obtained for glucose oxidation after subtracting the background (the response in absence of glucose) is proportional to the square root of the scan rate (Fig. 7B), indicating a typical behavior for a mass transfer controlled reaction. The slope increases in the order; 200 > 400 > 600 °C. The peak current, j_p of diffusion-controlled totally irreversible process can be given by Randles–Sevcik equation (Eq. (7)) [41]:

$$j_p = 2.99x10^5 n\ (\alpha\, n_a)^{0.5} A\, C (D\nu)^{0.5} \quad (7)$$

where j_p is the peak current (A), n is the total number of electrons, α is the charge transfer coefficient, n_a is the number of electrons in the rate determining step ($n_a = 1$), A is the surface area of the

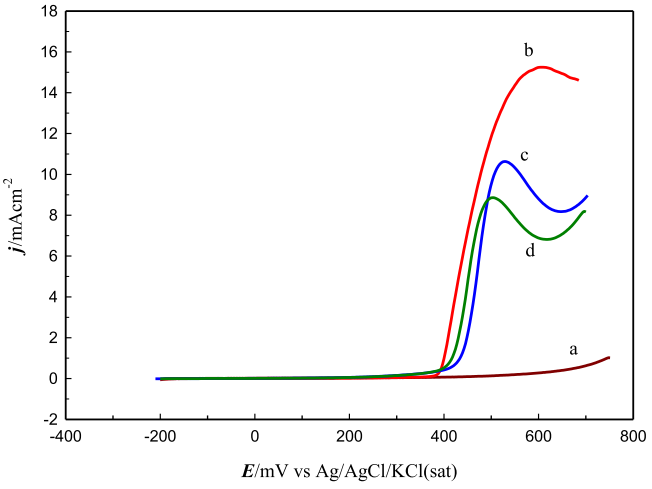

Fig. 5. LSVs for glucose oxidation obtained at (a) bare GC, (b–d) nano-NiO_x/GC electrodes in 0.3 M KOH containing 10 mM glucose at a scan rate 100 mVs^{-1}. The NiO_x were calcined at (b) 200, (c) 400 and (d) 600 °C. NiO_x loading is 0.14 mg cm^{-2}.

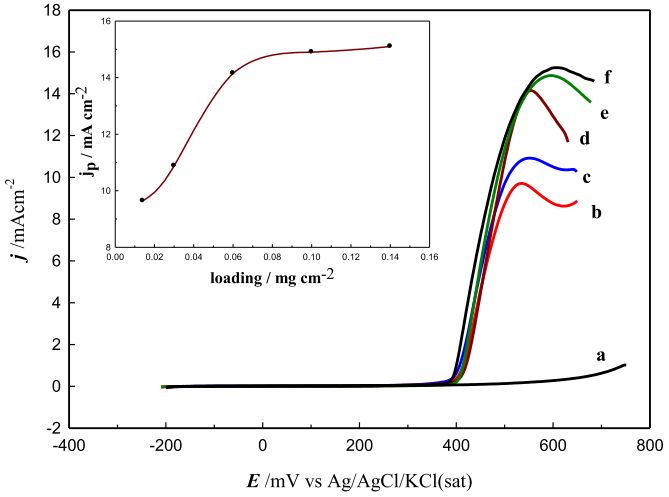

Fig. 6. LSV for glucose oxidation obtained at nano-NiO_x/GC electrode in 0.3 M KOH solution containing 10 mM glucose at a scan rate of 100 mVs^{-1}. The loading of NiO_x: (a) 0.0 (bare GC), (b) 0.014, (c) 0.03, (d) 0.06, (e) 0.10 and (f) 0.14 mg cm^{-2}. Inset shows the variation of j_p of glucose oxidation with the loading extent.

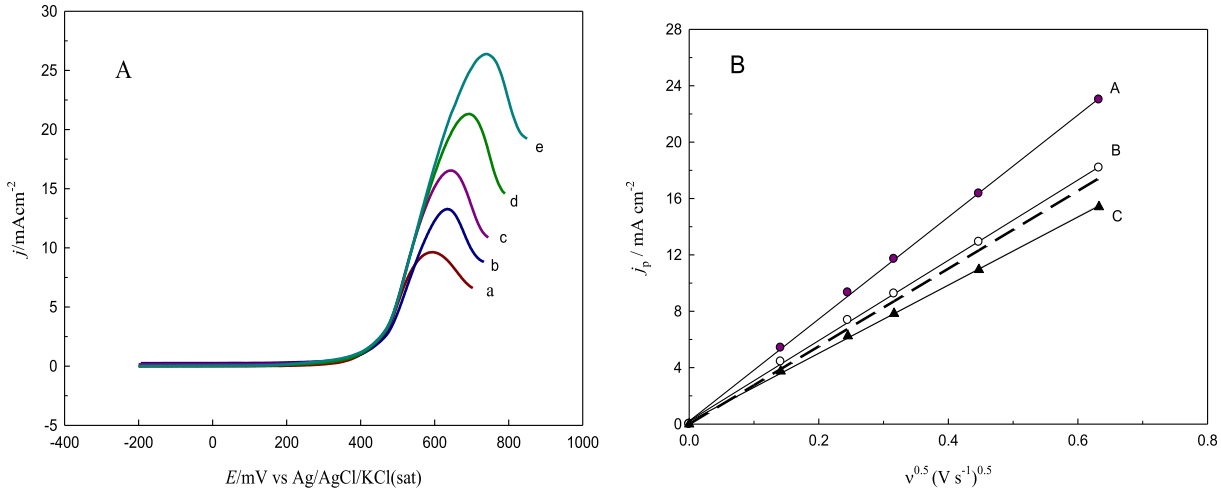

Fig. 7. A) LSV responses obtained at nano-NiOx/GC electrode in 0.3 M KOH solution containing 10 mM glucose. Potential scan rate: (a) 20, (b) 60, (c) 100, (d) 200, (e) 400 mVs^{-1}. The NiO_x was calcined at 200 °C. B) The variation of j_p with square rate of the scan rate obtained at nano-NiOx/G electrode in 0.3 M KOH containing 10 mM glucose at different calcination temperatures: (a) 200 °C, (b) 400 °C and (c) 600 °C. Dashed line shows Randles–Sevcik Theoretical plot for irreversible process given by Eq. 7

working electrode (cm^2), D is the diffusion coefficient of the glucose, C is the bulk concentration of the glucose and v is the scan rate (V s^{-1}). The theoretical plot based on Randles–Sevcik equation is given in Fig. 7B (dashed line). It was calculated using values of $D = 6.7 \times 10^{-6}$ cm^2 s^{-1} [53], $A = 0.07$ cm^2 and $\alpha = 0.59$ (as calculated from the slope of Tafel plot given in Fig. 8). As clearly shown Randles–Sevcik equation is strictly followed indicating a diffusion controlled process. However, theoretical values of j_p are not exactly equal to the experimentally determined values. It is noteworthy to mention that the enhancement of glucose oxidation at the present modified electrode is either similar or superior, in term of current and/or peak potential, to those reported at nickel oxide modified electrodes in same medium [54–58].

Fig. 8 depicts Tafel plots derived from a current–potential curve obtained at nano-NiO_x/GC annealed at 200 °C (A), 400 °C (B) and 600 °C (C) in the presence of 5 mM glucose using scan rate of 20 mV s^{-1} electrode. The plots demonstrate the enhancement of the glucose oxidation on nano-NiO_x/GC annealed at 200 °C compared to that annealed at the other temperatures. Tafel slope estimated from the plots is 130 mV/dec (±3 mV) for the nano-NiO_x/GC annealed at the different temperatures. This indicates that the mechanism of glucose oxidation does not change on the different electrodes and it is one-electron controlled process (see Eqs. (5) and (6)). Several values for the Tafel slope based on the modification of the electrode and the underlying substrate in the case of the same modifier have been reported [59–63]. For example at nickel oxide modified electrodes Tafel slopes equals 167.5 and 128.3 mV decade^{-1} for nickel oxide modified carbon nanotube and glassy carbon, respectively, have been reported [59,60]. A value of 120 mV decade^{-1} has been reported at porous Cu film deposited on a Pt/Ti/Si [61], 98 mV decade^{-1} on gold nanowire array and 63 mV decade^{-1} on Fe_2O_3 nanowire arrays [62]. A value around 120 mV, as in the present case, indicates that one electron process is participating in the rate determining step, while a one around 60 mV decade-1 indicates two electrons are participating in the rate determining step. In the present case the value of 120 mV decade indicates that a one-electron transfer would be the rate-limiting step.

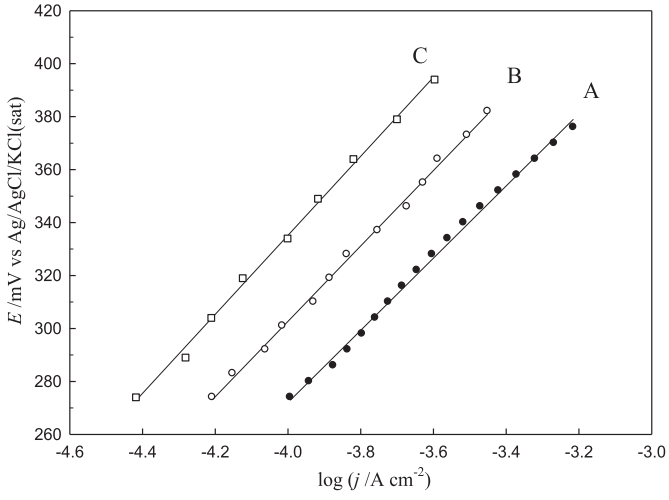

Fig. 8. Tafel plots for nano-NiO_x/GC electrode in 0.3 M KOH containing 5 mM glucose at a scan rate 20 mV/s. The NiO_x was calcined at 200 (A), 400 (B) and 600 °C (C). NiO_x loading is 0.06 mg cm^{-2}.

4. Conclusions

Glassy carbon electrode modified by casting nickel oxide nanoparticles prepared by sol–gel technique (nano-NiO_x/GC) has been used for glucose electrooxidation in alkaline solution. The impacts of annealing temperature of NiO_x powder and the loading extent on the structural and electrocatalytic properties of Nano-NiO_x/GC were studied. The followings could be extracted from this piece of work;

1. The calcination temperature of nano-NiO_x played a prominent role in the structural and electrocatalytic properties of the prepared nano-NiO_x.
2. The electrocatalytic activity of nano-NiO_x/GC towards glucose electrooxidation increases with increasing loading of nano-NiO_x with a pronouncing effect of loading.
3. A trial was introduced for optimization of the annealing temperature and loading extent under the prevailed experimental conditions.

References

[1] B. Sheela, H. Gomathi, G.P. Rao, J. Electroanal. Chem. 394 (1995) 267.
[2] K. YuanHwa, B. Subramani, Biosens. Bioelectron. 62 (2014) 127–133.

[3] C.R. Makkus, K. Hemmes, D.W. Wir, J. Electrochem. Soc. 141 (1994) 3429.
[4] H. Teymourian, A. Salimi, S. Firoozi, A. Korani, S. Soltanian, Electrochim. Acta 143 (2014) 196–206.
[5] Zh Jiao, M. Wu, Zh Qui, H. Xu, Nanotechnology 14 (2003) 458.
[6] M. Muti, A. Erdema, Ayfer, A. Caliskan, T. Sınagc, Yumak, Colloids Surf. B Biointerfaces 86 (2011) 154–157.
[7] X.Y. Deng, Z. Chen, Mater. Lett. 58 (2004) 276.
[8] H. Mohebbi, T. Ebadzadeh, F.A. Hesari, J. Power Sources 178 (2008) 64.
[9] L. Xiang, X.Y. Deng, Y. Jin, Scr. Mater. 47 (2002) 219.
[10] J. Li, B. Xiao, L. Du, R. Yan, T.D. Liang, J. Fuel Chem. Technol. 36 (2008) 42.
[11] Y.S. Yoom, J.M. Im, D.W. Shin, Ceram. Int. 34 (2008) 873.
[12] D. Ai, X. Dai, Q. Li, C. Deng, S. Kang, China Particuol. 2 (2004) 157.
[13] C. Xu, K. Hang, S. Liu, G. Wang, X. Zhao, J. Cryst. Growth 255 (2003) 308.
[14] Ying Wu, Yiming He, Tinghua Wu, Weizheng Weng, Huilin Wan, Mater. Lett. 61 (2007) 2680.
[15] S. Krompiec, J. Mrowiec, K. Bialōn, A. Skutil, L. Dukowicz, A.B. Pajak, Jarzebski, J. Non. Cryst. Solids 315 (2003) 297.
[16] A. Kaddouri, E. Tempesti, C. Mazzocchia, Mater. Res. Bull. 39 (2004) 695.
[17] A. Vargas, C. Maldonado, J.A. Montoya, L. Noreña, J. Morales, Appl. Catal. A Gen. 273 (2004) 269.
[18] S. Natesakhawat, R.B. Watson, X. Wang, U.S. Ozkan, J. Catal. 234 (2005) 496.
[19] S. Natesakhawat, O. Oktar, U.S. Ozkan, J. Mol. Catal. A Chem. 241 (2005) 133.
[20] S. Pilban Jahromi, N.M. Huang, M.R. Muhamad, H.N. Lim, Ceram. Int. 39 (2013) 3910.
[21] V. Patil, S. Pawar, M. Chougole, P. Godse, R. Sakhare, S. Sen, P. Joshi, J. Surf. Eng. Mat. Adv. Technol. (2011) 37.
[22] S.G. Pawar, M.A. Chougule, P.R. Godse, D.M. Jundale, S.A. Pawar, B.T. Raut, V.B. Patil, J. Nano Electron. Phys. 3 (1) (2011) 191.
[23] Ying Wu, Yiming He, Tinghua Wu, Tong Chen, Weizheng Weng, Huilin Wan, Mater. Lett. 61 (2007) 3176.
[24] A. Heller, B. Feldman, Chem. Rev. 108 (2008) 2482. Washington, DC, U.S.
[25] W. Loeb, Biochem. Z. 17 (1909) 132.
[26] M. Pasta, R. Ruffo, E. Falletta, C.M. Mari, C. Della Pina, Gold Bull. 43 (1) (2010).
[27] Y.B. Vasilév, O.A. Khazova, N.N. Nikolaera, J. Electroanal. Chem. Interfacial Electrochem. 196 (1985) 127.
[28] M. Vidotti, V.D. Cerri, R.F. Carvalhal, J.C. Dias, R.K. Mendes, S.I. Córdoba de torresi, L.T. Kubota, J. Electroanal. Chem. 636 (2009) 18.
[29] C. Li, Y. Liu, L. Li, Z. Du, S. Xu, M. Zhang, X. Yin, T. Wang, Talanta 77 (2008) 455.
[30] S. Berchmans, H. Gomathi, G. Prabhakara Rao, J. Electroanal. Chem. 394 (1995) 267.
[31] L.-C. Jiang, W.D. Zhang, Biosens. Bioelectron. 25 (2010) 1402.
[32] D. Das, P.K. Sen, K. Das, Electrochim. Acta 54 (2008) 289.
[33] Ying Wu, Yiming He, Tinghua Wu, Weizheng Weng, Huilin Wan, Mater. Lett. 61 (2007) 2680.
[34] C. Hu, Z. Gao, X. Yang, J. Sol Gel Technol. 44 (2007) 171.
[35] J.V. Smith (Ed.), X-ray Powder Data File, American Society for Testing Materials, 1960.
[36] Gu Feng, S.F. Wang, M.K. Lu, G. J Zhou, D. Xu, D.R. Yuan, J. Phys. Chem. B 108 (2004) 8119.
[37] X. Yang, J. Sun, Y. Wang, J. Yang, J. Mol. Catal. A Chem. 252 (2006) 17–22.
[38] D. Giovanelli, N.S. Lawrence, L. Jiang, T.G.J. Jones, R.G. Compton, Sens. Actuators B Chem. 88 (2003) 320.
[39] D. Giovanelli, N.S. Lawrence, S.J. Wilkins, L. Jiang, T.G.J. Jones, R.G. Compton, Talanta 61 (2003) 211.
[40] J. Wang, Analytical Electrochemistry, VCH Publisher Inc., New York, 1994.
[41] A.J. Bard, L.R. Faulkner, Electrochemical Methods: Fundamentals and Applications, Wiley, New York, 1980.
[42] S.M. El Refaei, M.I. Awad, B.E. ElAnadouli, M.M. Saleh, Electrochim. Acta 92 (2013) 463.
[43] S. Berchmans, H. Gomathi, G.P. Rao, J. Electroanal. Chem. 394 (1995) 267.
[44] J.R. Allen, A. Florido, S.D. Young, S. Daunert, L.G. Bachas, Electroanalysis 7 (1995) 710.
[45] I.G. Casella, T.R.I. Cataldi, A.M. Salvi, E. Desimoni, Anal. Chim. Acta 248 (1993) 3143.
[46] R.D.L. Smith, M.S. Prevot, R.D. Fagan, S. Trudel, C.P. Berlinguette, J. Am. Chem. Soc. 135 (2013) 11580.
[47] X. Zhou, Z. Xia, Z. Zhang, Y. Ma, Y. Qu, J. Mater. Chem. A 2 (2014) 11799.
[48] S. Berchmans, H. Gomathi, G.P. Rao, J. Electroanal. Chem. 394 (1995) 267.
[49] H. Heli, M. Jafarian, M.G. Mahjani, F. Gobal, Electrochim. Acta 49 (2004) 4999.
[50] B.E. Hayden, D. Pletcher, J. Suchsland, L.J. Williams, Phys. Chem. Chem. Phys. 11 (2009) 9141.
[51] T. Chen, S.C. Barton, G. Binyamin, Z. Gao, Y. Zhang, H.H. Kim, A. Heller, J. Am. Chem. Soc. 123 (2001) 8630.
[52] Y. Ding, Y. Liu, J. Parisi, L. Zhang, Y. Lei, Biosens. Bioelectron. 28 (2011) 393.
[53] M.Y. Elahi, H. Heli, S.Z. Bathaie, M.F. Mousav, J. Solid State Electrochem. 11 (2007) 273.
[54] W. Lu, X. Qin, A.M. Asiri, A.O. Al-Youbi, X. Sun, Analyst 138 (2013) 429.
[55] F. Gao, S. Guo, H. Ma, D. Shan, S. Yang, J. Gong, Biosens. Bioelectron. 26 (2011) 2756.
[56] Y. Ding, Y. Liu, L. Zhang, Y. Wang, M. Bellagamba, J. Parisi, C.M. Li, Y. Lei, Electrochim. Acta 58 (2011) 209.
[57] K.E. Toghill, R.G. Compton, Int. J. Electrochem. Sci. 5 (2010) 1246.
[58] K.-C. Lin, Y.-C. Lin, S.-M. Chen, Electrochim. Acta 96 (2013) 164.
[59] M. Shamsipur, M. Najafi, M.-R.M. Hosseini, Bioelectrochemistry 77 (2010) 120.
[60] A.C. de Sá, L.L. Paim, N.R. Stradiotto, Int. J. Electrochem. Sci. 9 (2014) 7746.
[61] S. Cherevko, C.-H. Chung, Talanta 80 (2010) 1371.
[62] S. Cherevko, C.-H. Chung, Sens. Actuators B 142 (2009) 216.
[63] S. Berchmans, H. Gomathi, G.P. Rao, J. Electroanal. Chem. 394 (1995) 267.